ELSEVIER

Polymer 42 (2001) 9173–9185

polymer

www.elsevier.com/locate/polymer

Morphology development during polymerization-induced phase separation in a polymer dispersed liquid crystal

Thein Kyu*, Hao-Wen Chiu

Institute of Polymer Engineering, University of Akron, Akron, OH 44325, USA

Received 2 March 2001; received in revised form 4 April 2001; accepted 4 April 2001

Abstract

To elucidate the emergence of liquid crystal (LC) domains during polymerization induced phase separation in a polymer dispersed liquid crystal (PDLC), numerical simulation has been performed by incorporating the kinetics of crosslinking reaction into the time-dependent Ginzburg–Landau (TDGL-Model C) equations in conjunction with the combined Flory–Huggins (FH)/Maier–Saupe (MS) free energies. The TDGL-Model C basically consists of two coupled equations in which a conserved compositional order parameter (i.e. the volume fraction) is coupled with a non-conserved orientational order parameter of the LCs. Of particular interest is the influence of nematic ordering on the emergence of domain morphology that shows a strong dependence on curing temperatures and compositions, displaying a rich variety of patterns.

Keywords: Polymerization-induced phase separation; Reaction–diffusion equation; Nematic ordering

1. Introduction

The electro-optical performance of polymer-dispersed liquid crystal (PDLC) devices involving fast on–off switching time, low driving voltage, high contrast in on-state transmittance and off-state opacity depends strongly on the shape, size, and uniformity of the dispersed liquid crystal (LC) domains [1–3]. Basically PDLC is an inhomogeneous composite film comprised of low molar mass LC dispersion in a polymer matrix. Phase separation techniques such as thermally induced phase separation (TIPS) or polymerization (or photopolymerization) induced phase separation (PIPS) of the reactive matrix (often called polymer binder) have been generally employed to fabricate the PDLC films [3]. In the former case of TIPS, the instability of the PDLC system is driven by the competition between phase separation and nematic ordering. As for the latter case, the instability is induced by an increase in molecular weight of the starting reactive monomers that eventually results in phase separation between LCs and emerging polymers.

It has been recognized that the final LC domain morphology depends not only on thermodynamic phase equilibria of the LC/polymer mixtures, but also depends strongly on dynamics of phase decomposition and nematic ordering as most polymer systems rarely reach an equilibrium state [4,5]. In our previous papers [6–11], we dealt with theoretical elucidation and experimental determination of the equilibrium phase diagrams of various PDLC systems. The combination of the free energies of Flory–Huggins (FH) theory for isotropic mixing [12,13] and Maier–Saupe (MS) theory for nematic ordering [14–16] or Maier–Saupe–McMillan (MSM) theory for smectic ordering [17] has been shown to be useful in explaining the observed PDLC phase diagrams.

Regarding dynamics of phase separation, early theoretical attempts have focused on simulation of the dynamics of PIPS in nematic LC/polymer mixtures were undertaken in the isotropic state without taking into consideration the isotropic–nematic transition [18–27]. Many research groups [28–34] including us [6–11] have demonstrated the significance of nematic ordering on the phase diagrams of LC/polymer systems, hence it can be anticipated that the nematic ordering would play an equally import role in the morphology development. Recently, the coupled time-dependent Ginzburg–Landau (TDGL-Model C) equations have been utilized [35–40] to mimic the dynamics of phase separation in liquid crystalline polymer solutions [35,36] and LC/polymer mixtures [38–40]. The Model C equations are basically two coupled equations in which a conserved compositional (concentration) order parameter is

* Corresponding author. Present address: Essilor of America, Inc., Optical Thermoplastics R & D, St Petersburg, FL 33709, USA. Tel.: +1-330-972-6865; fax: +1-330-258-2339.

E-mail address: tkyu@uakron.edu (T. Kyu).

0032-3861/01/$ - see front matter
PII: S0032-3861(01)00389-5

coupled with a non-conserved orientational order parameter of the LC directors. The aforementioned TDGL approach has been applied to some thermal quench PDLC systems in which the emerging morphologies have been explained on the basis of the competition between the phase separation dynamics and nematic ordering by Lapena et al. [38] and Fukuda [39,40]. The advantage of their approach [38–40] over others [36,37,41] is that the coefficients of the nematic curvature gradient were treated in a tensorial form by taking into consideration the anisotropic nature of LC molecules, therefore it is more rigorous. However, one drawback of the tensorial approach is that it is impractical to experimentally determine the individual elements of these coefficient tensors of the curvature gradient. The tensorial approach may be simplified as demonstrated by Dorgan and Yan [36], Lin et al. [37] as well as by us [41] who employed the scalar coefficient of the nematic curvature gradient. Recently, Model C has been applied to elucidate the emergence of morphology in photo-initiated PIPS of an LC/polymer mixture [42].

In our recent paper [41], the morphology development and the dynamics of phase transitions, associated with thermal quenching in a nematic/polymer mixture, have been solved numerically on the basis of the time-dependent Ginzburg–Landau (TDGL) equations, i.e. 'Model C', in conjunction with the combined Flory–Huggins/Maier–Saupe free energies. An unusual plateau region in the coarsening dynamic curves was observed in the simulation. This unique behavior has been verified experimentally in the blends of nematic LC/poly(methyl methacrylate) as evidenced by time-resolved light scattering [43,44]. In this plateau region, the interconnected phase separated domains are seemingly broken down to droplet morphology. This region incidentally corresponds to the onset of the nematic ordering.

As a continuing effort, the emergence of LC domain morphology within a PDLC prepared via thermally initiated PIPS is investigated. The mechanisms on polymerization kinetics of homopolymers involving condensation, emulsion polymerization, free radical polymerization, etc. have been well established [45]. However, the relationship between synthesis and the emerging domain morphology of the multicomponent system is relatively misunderstood because of the complex phase separation occurring during polymerization [45–49]. In particular, the interplay of polymerization kinetics, dynamics of phase separation and nematic ordering of the LC molecules needs to be resolved. By incorporating the reaction kinetics into the coupled TDGL equations in conjunction with the combined FH/MS theory, the pattern forming aspect of phase separation driven by progressive polymerization has been solved numerically. Of particular interest is our simulation shows a variety of LC domain morphologies in a manner dependent on the trajectory of the coexistence curve relative to the reaction temperature and composition during polymerization-induced phase separation.

2. Model description

2.1. Phase equilibrium

The isotropic part of the free energy is generally described in terms of the Flory–Huggins (FH) theory [12,13], i.e.

$$g^{\mathrm{i}} = \frac{\phi_1}{N_1}\ln\phi_1 + \frac{\phi_2}{N_2(t)}\ln\phi_2 + \chi\phi_1\phi_2 \tag{1}$$

where χ is the Flory–Huggins interaction parameter defined as $\chi = A + B/T$ with A and B being constants [13].

The anisotropic part of the free energy may be given according to the Maier–Saupe (MS) theory [14–16]

$$g^{\mathrm{n}} = \tfrac{1}{2}\nu s^2\phi_1^2 - \phi_1\ln Z \tag{2}$$

where ν is the nematic interaction parameter defined as $\nu = 4.541(T_{\mathrm{NI}}/T)$ [6,7] in which T_{NI} is the nematic–isotropic (NI) transition temperature of the LC component. Z is the partition function given as

$$Z = \int_0^1 \mathrm{e}^{\nu s\phi_1((3/2)\cos^2\theta - 1/2)}\mathrm{d}\cos\theta \tag{3}$$

and s is the nematic order parameter defined as

$$s = \frac{1}{2}\langle 3\cos^2\theta - 1\rangle$$

$$= \frac{\int_0^1((3/2)\cos^2\theta - 1/2)\mathrm{e}^{\nu s\phi_1((3/2)\cos^2\theta - 1/2)}\mathrm{d}\cos\theta}{Z} \tag{4}$$

The nematic–isotropic transition may be determined by minimizing the free energy of anisotropic ordering with respect to the order parameter, s, i.e. $\partial g^{\mathrm{n}}/\partial s = 0$. at $s = s_{\mathrm{c}}$. The critical orientational order parameter s_{c}, which is defined as the threshold value to form a stable nematic phase at a given concentration, i.e. the liquid crystalline phase is unstable below this critical point, but stable above it, i.e. $s_{\mathrm{c}} \le s \le 1$. Once the temperature dependence of the order parameters has been determined, the free energy of anisotropic ordering can be calculated accordingly. The equilibrium coexistence points of the phase diagram can then be computed by using a double tangent method [6,7] or by minimizing the total free energy with respect to concentration, ϕ such that the chemical potentials of the individual phase are equivalent. Regarding the details of phase diagram calculation, interested readers are referred to our previous paper [6–11].

2.2. Phase separation dynamics and nematic ordering

The emergence of (LC) domains in a polymer dispersed liquid crystal (PDLC) system prepared via polymerization induced phase separation (PIPS) may be treated as a reaction–diffusion process coupled with the nematic ordering of the LC molecules. The system under consideration is a PDLC system in which only one component (i.e. matrix

monomer) is involved in the reaction, i.e. the crosslinking reaction occurs in the reactive monomer in the presence of the non-reacting LC component. The phase separation dynamics of such a dissipative system may be described by incorporating the reaction kinetics into the coupled TDGL-Model C equations [4,5,35–41] in which the compositional order parameters, i.e. the volume fractions of LC, monomer, and emerging polymer, are coupled with a non-conserved orientational order parameter of the LC as follows:

$$\frac{\partial \phi_1(r,t)}{\partial t} = -\nabla \cdot J_1 + \eta_1(r,t) \tag{5}$$

$$\frac{\partial s(r,t)}{\partial t} = -R\left(\frac{\delta G}{\delta s}\right) + \eta_s(r,t) \tag{6}$$

where G is the total free energy density of the system, t is time in dimensionless units and R is related to the rotational mobility of the LC molecules [35]. When polymerization proceeds, the monomers convert to a polymer, therefore the monomer concentration decreases. The change of monomer and polymer concentrations may be expressed in terms of the reaction–diffusion equations in what follows:

$$\frac{\partial \phi_m(r,t)}{\partial t} = -\nabla \cdot J_m - \dot{\alpha}(t)\phi_m(r,t) + \eta_m(r,t) \tag{7}$$

$$\frac{\partial \phi_p(r,t)}{\partial t} = -\nabla \cdot J_p + \dot{\alpha}(t)\phi_m(r,t) + \eta_p(r,t) \tag{8}$$

with

$$\phi_1 + \phi_m + \phi_p = 1 \tag{9}$$

where $\phi_1(r,t)$, $\phi_m(r,t)$ and $\phi_p(r,t)$ are the volume fractions of the non-reacting LC, the monomer, and the resulting polymer at position r and reaction time t, respectively. $s(r,t)$ is the orientational order parameter of the LC component. J_k ($k = l$, m, and p) is the flux of component k. $\eta_k(r,t)$ and $\eta_s(r,t)$ are the concentration and orientation fluctuations, respectively, that satisfy the fluctuation-dissipation theorem. $\dot{\alpha}(t)$ is the rate of monomer conversion.

The reaction kinetics for cure reaction induced phase separation of a rubber modified epoxy system has been treated empirically in polymer chemistry [45,51] according to Eq. (10). We extended this equation to describe the spatio-temporal growth of phase separated domains in rubber modified epoxy subjected to PIPS [23]. Later, Chan and Rey [25] employed a simpler version of the same equation in the simulation of the morphology development in an isotropic mixture based on an idealized assumption of reaction-driven phase separation. For a generalized curing reaction involving a thermosetting resin and a curing agent, the reaction kinetics is expressed as [23,48]

$$\dot{\alpha}(t') = \frac{\mathrm{d}\,\alpha(t')}{\mathrm{d}t'} = k'(T)\alpha(t')^m[1-\alpha(t')]^n \tag{10}$$

and k' is the rate constant in units of reciprocal time. Note that t' and k' may be non-dimensionalized in the simulation. m and n are reaction kinetic exponents characterizing the growth of polymer chains and the rate of monomers consumed, respectively. $k'(T)$ is the reaction rate constant that depends on reaction temperature, which may be described in the framework of Arrhenius form, viz. $k'(T) = k_0 \exp(-E_0/k_B T)$. The degree of conversion (i.e. the functional sites reacted relative to the total functional groups), $\alpha(t')$, may be expressed according to the Carother's equation [44]

$$\alpha(t') = \frac{2(M_0 - M)}{M_0 f_{av}} \tag{11}$$

where the average functional group that has been reacted is defined as $f_{av} = \sum M_j f_j / \sum M_j$. M_j is the number of molecules of monomer j having functionality f_j, M_0, the number of monomer molecules, and M, the number of molecules reacted. The degree of polymerization is given as $N_2 = M_0/M$ which can be related to the degree of conversion as follow [44]:

$$N_2(t') = \frac{1}{1 - (1/2) f_{av}\alpha(t')} \tag{12}$$

The time-dependent expression of the degree of conversion in Eq. (12) permits the degree of polymerization to increase progressively with reaction time. As will be shown later, the increasing molecular weight of the reacting polymer causes the system to be unstable and eventually drives phase separation. The values of f_{av} vary from a value of two for a linear chain growth and three or higher for a crosslinking reaction depending on the functional sites of the curing agent employed. In the present case, f_{av} has been taken to be three, since a complete conversion cannot be expected for any crosslinking reaction [43].

When the polymerization rate is slow as compared to the kinetics of phase separation, a sizable amount of monomers would remain unreacted at a given time. In principle, the emerging polymer could segregate from the residual monomer as well as from the non-reacting LC component. Hence, such a reacting blend should be treated as a three-phase system as it contains the residual monomer, the emerging polymer, and the LCs. The pattern forming aspect for such a three-phase system may be modeled by numerically solving Eqs. (5)–(7) and (10) simultaneously. On the other hand, if the polymerization rate is faster than the kinetics of phase separation, most of the monomers will be consumed during polymerization. It can be anticipated that the emerging polymers may result in a wide distribution of molecular weights. As is well known, the molecular weight distribution exerts profound effect on the establishment of thermodynamic phase diagrams. However, the polydispersity plays an insignificant role in the phase separation dynamics of the thermal-quenched case [50] because of the wavelength selection, i.e. only a dominant single wavelength will be selected by the system during phase

separation. Hence, it is reasonable to assume that the influence of molecular weight distribution on the dynamics of PIPS may be inconsequential.

Assuming that the residual oligomers and the emerging polymers are completely miscible, the polymerizing component may be treated as a single component (hereafter designated as component 2 and $\phi_2 = \phi_m + \phi_p$), which further simplifies the treatment of the polymerizing system as a pseudo two-phase blend. Combining Eqs. (7) and (8) together along with the incompressibility condition, $\phi_1 + \phi_2 = 1$, one obtains

$$\frac{\partial \phi_2(r,t)}{\partial t} = -\nabla \cdot J_2 + \eta_2(r,t) \tag{13}$$

It is evident that Eq. (13) is complementary to Eq. (5). Hence, it should be sufficient to solve only three coupled equations (i.e. Eqs. (5), (6) and (10)) simultaneously in describing the dynamics of phase separation in a PDLC, in which only one component is reactive. On the basis of the aforementioned assumption, the diffusion flux J_1 in Eq. (5) is given by

$$J_1 = -\frac{\Lambda}{k_B T} \nabla \left[\frac{\delta G}{\delta \phi_1} \right] \tag{14}$$

where k_B is the Boltzmann constant and T is the absolute temperature. The mutual diffusion coefficient Λ having the property of the Onsager reciprocity [36] for a binary system is generally given as $\Lambda = \Lambda_1 \Lambda_2/(\Lambda_1 + \Lambda_2)$ with $\Lambda_1 = \phi N_1 D_1$ and $\Lambda_2 = (1-\phi) N_2(t) D_2$. Here N_1 represents the degree of polymerization of the dispersing LCs and $N_2(t)$ is that of the polymerizing component 2. D_1 and D_2 are the self-diffusion coefficients of the LC molecules and the polymer chains, respectively. In the framework of reptation theory [51], it may be expressed as

$$D_2 = \frac{k_B T}{\zeta_2} \frac{N_{e,2}}{N_2^2} \tag{15}$$

where ζ_2 and $N_{e,2}$ are the frictional coefficient per monomer unit and the distance between the entanglements of polymer chains, respectively.

The total free energy of the system, G, is given by the integration of the local free energy density over all volume, viz.

$$\frac{G}{k_B T} = \int_V (g^i + g^n + \kappa_\phi |\nabla \phi_1|^2 + \kappa_s |\nabla s|^2) \mathrm{d}V \tag{16}$$

where g^i is the free energy density of isotropic mixing and g^n is the free energy density due to the anisotropic ordering of the LC molecules. $\kappa_\phi |\nabla \phi_1|^2$ is the free energy of the concentration gradient in which κ_ϕ is a coefficient related to the segmental correlation length and the local concentration. For an asymmetric polymer–polymer mixture [52],

$$\kappa_\phi = \frac{1}{36} \left[\frac{a_1^2}{\phi_1} + \frac{a_2^2}{\phi_2} \right] \tag{17}$$

where a_1 and a_2 are the characteristic lengths of polymer segments of the component 1 and 2, respectively. The $\kappa_s |\nabla s|^2$ term in Eq. (16) represents the free energy gradient of the orientation order parameter. For simplicity κ_s may be taken as constant.

Based on the combined FH/MS free energy expression, Eqs. (5) and (6) lead to

$$\frac{\partial \phi_1}{\partial t} = \nabla \cdot \left[\Lambda \nabla \left(\frac{\partial g^i}{\partial \phi_1} + \frac{\partial g^n}{\partial \phi_1} - \kappa_\phi \nabla^2 \phi_1 \right) \right] + \eta_1 \tag{18}$$

$$\frac{\partial s}{\partial t} = -R \left(\frac{\partial g^n}{\partial s} - \kappa_s \nabla^2 s \right) + \eta_s \tag{19}$$

where

$$\frac{\partial g^i}{\partial \phi_1} = \frac{\ln \phi_1 + 1}{N_1} - \frac{\ln(1-\phi_1) + 1}{N_2(t)} + \chi(1 - 2\phi_1) \tag{20}$$

$$\frac{\partial g^n}{\partial \phi_1} = \nu s^2 \phi_1 - \ln Z - \phi_1 \frac{\partial \ln Z}{\partial \phi_1} \tag{21}$$

$$\frac{\partial g^n}{\partial s} = \nu s \phi_1^2 - \phi_1 \frac{\partial \ln Z}{\partial s} \tag{22}$$

The pattern forming aspects of phase separation within a PDLC system during polymerization may then be investigated by numerically solving Eqs. (10), (18) and (19) simultaneously. It should be pointed out that the molecular diffusion is coupled with the polymerization reaction through the time dependence of the molecular weight of the polymerizing component, $N_2(t)$, although the reaction rate term involving monomer conversion has been eliminated from the reaction–diffusion equations through the combination of Eqs. (7) and (8) leading to Eq. (13). In the event of a three-phase system consisting of the residual monomer (or oligomer), the emerging polymer, and the non-reacting LCs, the reaction and diffusion processes are coupled through both $N_2(t)$ and $\alpha(t)$. Hence the temporal change of concentration fluctuations would be dominated by both the change in the local free energy density (or chemical potential) driven by the progressive polymerization as well as by the coupling term involving the conversion rate, $\dot{\alpha}(t)$, and the monomer concentration.

The temporal evolution of structure factors, $S_\phi(q,t)$ and $S_s(q,t)$, may be determined by rewriting Eqs. (18) and (19) in Fourier space, i.e.

$$S_\phi(q,t) = F[\phi_1(r_1,t)\phi_1(r_2,t)] \tag{23}$$

$$S_s(q,t) = F[s(r_1,t)s(r_2,t)] \tag{24}$$

where F represents the Fourier transformation and q is the scattering wavenumber defined as $q = [4\pi/\lambda]\sin(\theta/2)$ where λ and θ are the wavelength of incident light and scattering angle in the medium, respectively. Numerical calculation was performed on a two-dimensional square lattice (128×128) using an explicit method for temporal steps and a

central difference scheme for spatial steps with a periodic boundary condition. Both the grid size and the time step were chosen sufficiently small to ensure that changes in them exerted little or no effect on the calculated results.

3. Results and discussion

3.1. Effect of polymerization on phase diagram

Fig. 1(a) illustrates the initial phase diagram of the reactive monomer/nematic LC mixture calculated on the basis of the combined FH/MS theory [6,7] using the following conditions: $T_{NI} = 80°C$,$N_2/N_1 = 1/1$ corresponding to the critical composition of the liquid–liquid coexistence curve of the starting mixture, $\phi_c = 0.5$, and the critical temperature, $T_c = 50°C$. The constant A of the χ parameter is set as $A = -5$, which in turn gives $B = 2262$ from the critical condition, i.e. $B = (\chi_c - A)T_c$. The calculated phase diagram is essentially an overlap of an upper critical solution temperature (UCST) and a NI transition, exhibiting a variety of coexistence regions such as isotropic liquid + isotropic liquid and nematic (N) + liquid (L) in the intermediate compositions. At very high LC rich compositions, the pure nematic and a narrow N + L region exists at high temperatures. Following the method of Shen and Kyu [6], the nematic–liquid (N–L) spinodal line has been calculated self-consistently as depicted in Fig. 1(a). The nematic spinodal line divides the narrow N + L region into the metastable nematic, $[M_N]$, and the unstable nematic, $[U_N]$, regions. As labeled in the phase diagram, the metastable nematic region is bound by the pure nematic and the nematic spinodal lines, whereas the unstable nematic region is bound by the nematic spinodal and the nematic–isotropic transition lines. Similarly, the liquid–liquid spinodal line divides the phase diagram into the unstable liquid, $[U_L]$, and metastable liquid, $[M_L]$, regions. To the best of our knowledge, Shen and Kyu [6] are the first to theoretically predict the nematic spinodal line. In support of Shen and Kyu approach [6], Matsuyama and Kato [31] independently calculated the spinodal limits of the NI as well as the smectic–isotropic transitions in the main-chain LC polymer solution. It should be emphasized that their calculated N–L spinodal line is strikingly similar to the present nematic spinodal line. Recently, our theoretical model [6] has been extended by Benmounna et al. [33] to the LC/polymer network system.

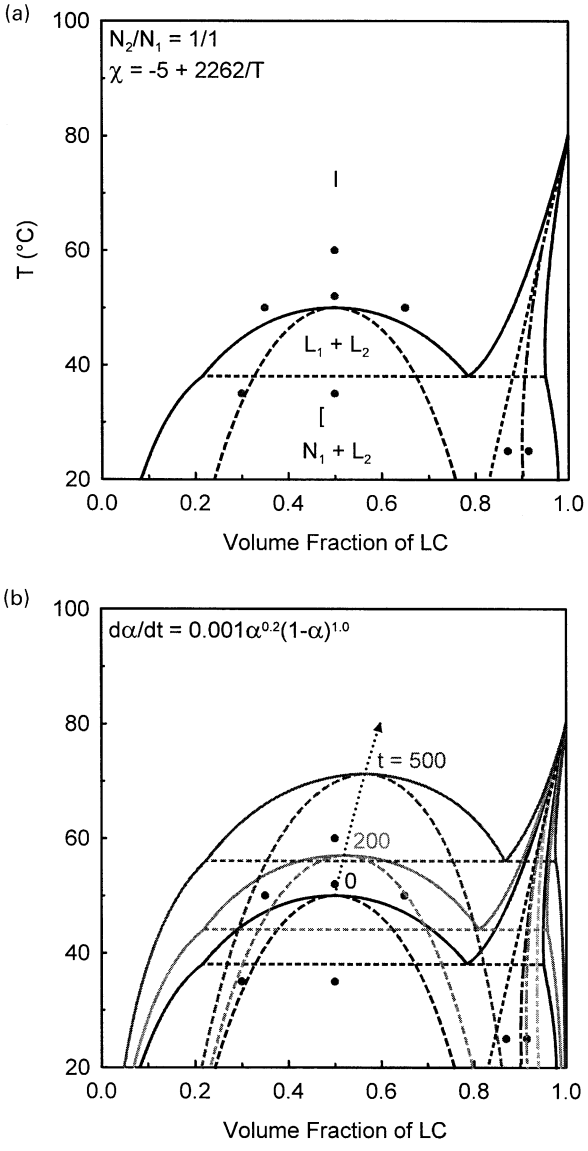

Fig. 1. (a) A hypothetical phase diagram of a monomer/nematic liquid crystal mixture, calculated on the basis of the combined FH/MS theory, displaying various coexistence regions. (b) Progressive movement of the phase diagram with increasing reaction time (or degree of polymerization). The filled circles indicate different compositions and reaction temperatures chosen for the simulation of the pattern forming process associated with polymerization.

As the polymerization advances, the molecular weight of component 2, $N_2(t)$ increases progressively which drives the UCST curve to shift asymmetrically to a higher temperature, but noticeably to a lower composition of the polymerizing component (i.e. the high LC side) with reaction time (Fig. 1(b)). Concurrently, the nematic–liquid spinodal line moves toward a higher LC content. However, the N–I transition line is unaffected by the polymerization. As will be shown later, the shift of the N–L spinodal line has profound influence on the emergence of the nematic domains during PIPS in a two-phase region.

3.2. Reaction in a single-phase region

3.2.1. Reaction at the critical composition in the starting mixture

We shall now examine the emergence of liquid crystal domains during the course of polymerization. The calculation was first performed for a case where polymerization was initiated in a single-phase region at a reaction temperature $T_R = 52°C$ and $\phi_1 = 0.5$ corresponding to the critical composition of the starting monomer/LC mixture along

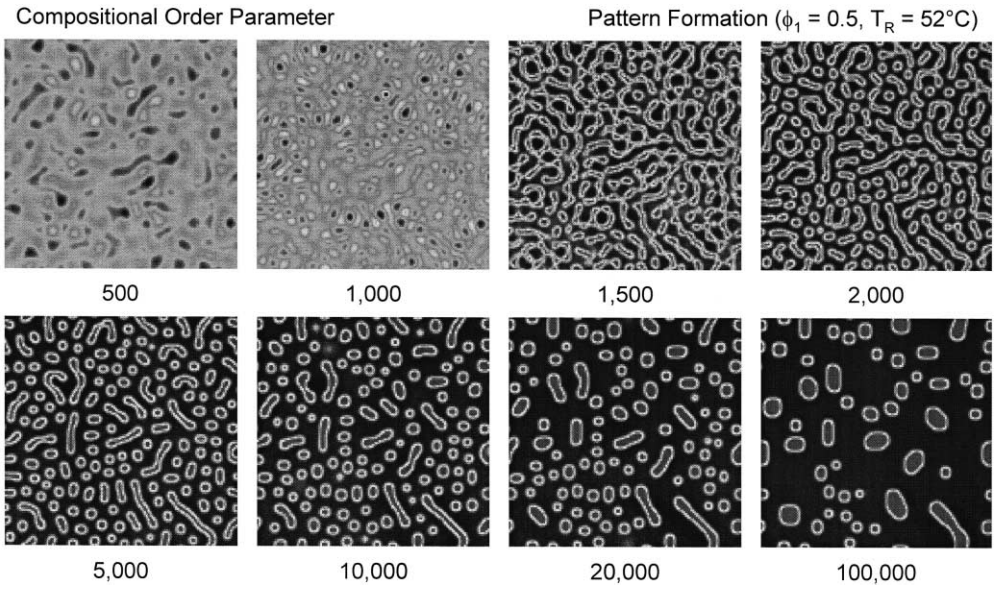

Fig. 2. Temporal evolution of the compositional order parameter for the case $\phi_1 = 0.50$ and the reaction temperature $T_R = 52°C$. The calculation was performed using the following parameters: $T_{NI} = 80°C$, $D_1 = D_2 = 0.2$, $a_1 = 1.6$, $a_2 = 1.6$, $R = 0.1$, $\kappa_s = 0.1$, and the reaction kinetic constants $k = 0.001$, $m = 0.2$, and $n = 1$.

with the reaction kinetic constants: $k' = 0.001$, $m = 0.2$, and $n = 1.5$ obtained experimentally for the curing of bisphenol-A epoxy. For the purpose of simulation, the reaction time, t', and the reaction kinetic coefficient, k', may be renormalized in dimensionless units, e.g. $x = x'/\ell$, $y = y'/\ell$, $t = (\Lambda/\ell^2)t'$ and $k = (\ell^2/\Lambda)k'$, where ℓ is the length scale. Fig. 2 shows the temporal evolution of the compositional order parameter during progressive polymerization of the reacting monomers. The smaller thermal fluctuations tend to diminish much faster than the larger ones during the so-called induction period.

As polymerization advances, the UCST curve shifts asymmetrically to a higher temperature. When the binodal curve surpasses the reaction temperature, phase separation starts in a metastable region and drifts rapidly to an unstable region. In liquid–liquid phase separation, it is well known that SD is an unstable process and thus even small concentration fluctuations can grow. In the nucleation process, all smaller modes of concentration fluctuations tend to diminish in the induction period. Consequently, the disproportionate amount of large fluctuations are left behind upon which nucleation occurs. During PIPS, the coexistence curve generally surpasses the reaction temperature at an off-critical point, thus the system should pass through a metastable region. Hence, the phase separation process naturally occurs through a nucleation process. Newer domains are seemingly formed between the existing ones and also the domain size gets smaller (see 500–1000 time steps of Fig. 2). Subsequently, the concentration fluctuations grow in magnitude and eventually transform from the sea-and-island type to a so-called bicontinuous structure reminiscent of a spinodal texture as the system drifts from the metastable to the unstable region ($t =$ 1500–2000). Since phase separation was triggered in the metastable region before drifting into the unstable spinodal region with continued polymerization, this mechanism was termed nucleation initiated spinodal decomposition (NISD) [23] in order to differentiate from the conventional nucleation and growth (NG) and SD mechanisms of the thermal quenched system. With the progression of time, the bicontinuous structure breaks down into smaller droplets, signifying the percolation-to-cluster transition. Then some droplets grow through at the expense of smaller ones.

Fig. 3 depicts the temporal evolution of the corresponding orientational order parameter. As mentioned in a previous paper [39], the emerging process of the morphology in a PDLC system involves a competition between the liquid–liquid phase separation and the nematic ordering of the LC molecules. In the present case, the LC component was initially in the isotropic state as polymerization was carried out in a single-phase temperature. According to the combined FH/MS theory [6,7], nematic ordering occurs only when the LC concentration exceeds a critical concentration, i.e. $\phi_{NI} \approx T/T_{NI}$. Hence, the initial stage of phase separation is primarily driven by the liquid–liquid spinodal due to the fact that the LC concentration in the phase-separated domains has yet to reach the critical concentration, ϕ_{NI}. Later, the LC directors start to align within the interconnected domains ($t = 1000$). When the LC concentration reaches ϕ_{NI}, nematic ordering takes place. Tiny LC droplets develop and fill the bicontinuous domains. Since nematic ordering takes place preferentially within those bicontinuous LC rich domains, it is reasonable to infer that the orientational order of LC lags behind the compositional order during PIPS initiated in a single-phase temperature.

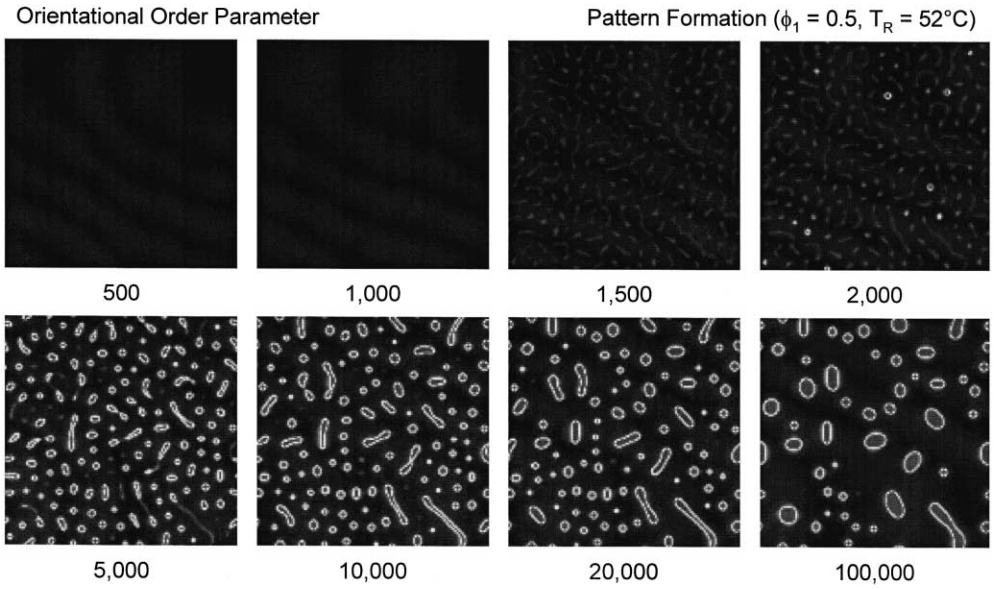

Fig. 3. Temporal evolution of the orientational order parameter obtained from the same calculation in Fig. 2.

Subsequently, the structure coarsens through coalescence ($t = 2000$–5000).

To further investigate the growth dynamics of PIPS, Fourier transformation was undertaken on the emerging domain structures depicted in the compositional order parameter field. The initial scattering pattern is small and very diffuse without a clear maximum, but the scattering pattern transforms to a diffuse halo (see $t = 500$ in Fig. 4). The diameter increases with progressive polymerization for some initial period (up to $t = 2000$), suggestive of reduction in the length scale. The increase in diameter of the scattering ring at $t = 1000$ may be attributed to the formation of newer domains between the existing ones or size reduction due to increasing supercooling during PIPS. When the LC ordering takes place, the interface seemingly gets sharper giving rise to a secondary scattering halo (1500–2000). As the polymerization continues, the structure factor intensifies while the size of the scattering ring collapses to a smaller diameter due to the structural coarsening ($t = 1500$–5000), presumably driven by thermal relaxation, i.e. $\mathcal{L} \propto t^{\gamma}$, which dominates over the size reduction due to increasing supercooling during PIPS, i.e. $\mathcal{L} \propto 1/\Delta T$.

The growth dynamics of PIPS in PDLC may be best characterized in term of a temporal scaling. As shown in Fig. 5, the initial rise in q_m (scattering wavenumber maximum) is due to decrease in the length scale, which

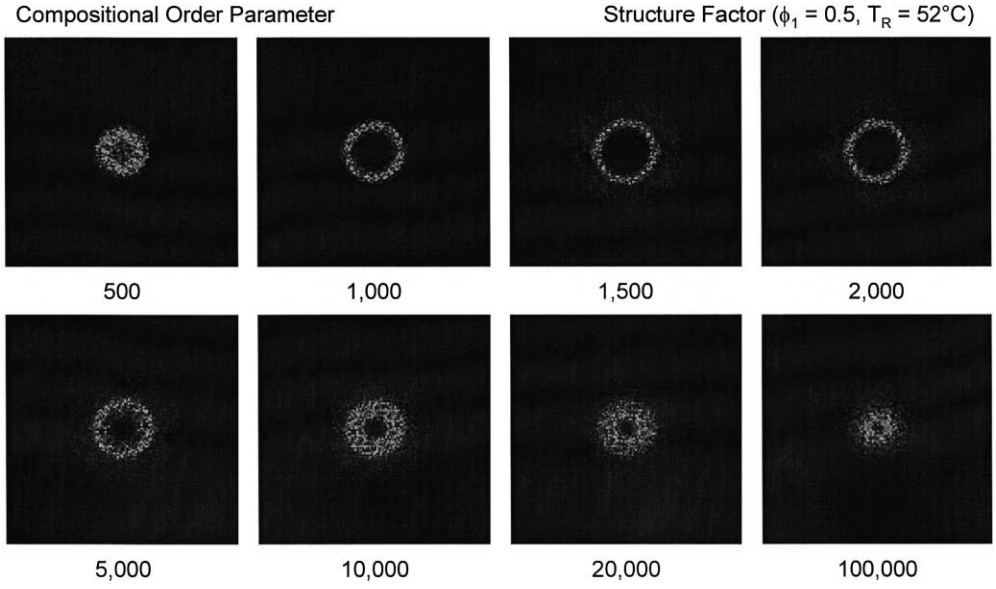

Fig. 4. Temporal evolution of the structure factor as obtained by Fourier transformation of the domain structure of the compositional order parameter field in Fig. 2.

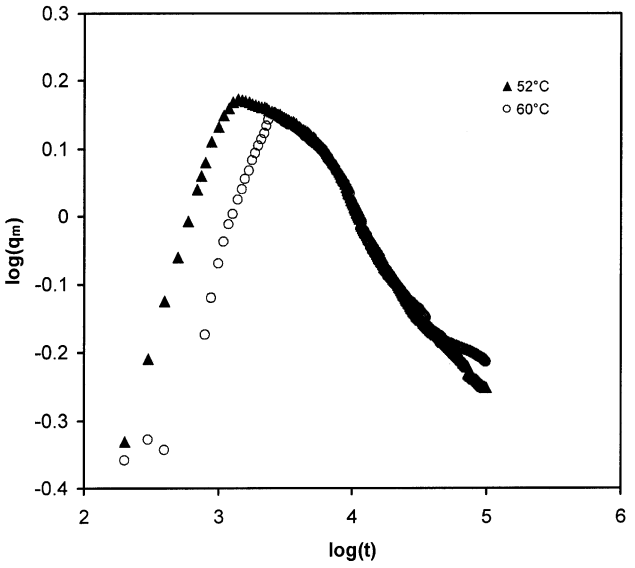

Fig. 5. $\log(q_m)$ versus $\log(t)$ plots for the compositional order parameter calculated for two different reaction temperatures of 52 and 60°C.

may be attributed to the increasing supercooling as the UCST coexistence curve shifts to a higher temperature beyond the reaction temperature, i.e. $q_m \propto \Delta T$. Then the scattering maximum falls off as the structural coarsening due to thermal relaxation, viz. $q_m \propto t^{-\gamma}$, becomes dominant. It is reasonable to infer that the growth dynamics of PIPS is determined by the competition between the size reduction due to increasing supercooling caused by the shift of the coexistence curve during PIPS and the structural coarsening due to the thermal relaxation.

When polymerization is initiated at a higher temperature of 60°C, the emerging patterns reveal a similar growth behavior, except that it takes a longer time for the PIPS process to catch-up with that at 52°C. In the intermediate to late stage of the growth regime, the two curves coincided with each other and the growth process continues. The growth curve of the orientational order parameter is virtually overlapped with that of the compositional order parameter, so the data are not presented here. The slope of the initial rise in q_m is approximately 1/2, but the slope changes its sign showing a subtle curvature, but in the narrow straight region a slope of $-1/3$ may be estimated. The initial rise may be interpreted as the reduction in length scale, but the physical meaning of 1/2 is presently unclear. Another concern regarding the interpretation of these growth exponents is their dependence on the dimensionality of growth. Since the present calculation was carried out in 2D, caution should be exercised in interpreting the meaning of the growth exponent, as it could be different from the 3D case. It appears that no universal law is valid for the entire growth region because of the competition between the two-opposing mechanisms: (i) the size reduction due to the increasing supercooling driven by the movement of the UCST, i.e. $q_m \propto \Delta T$ and (ii) the structural coarsening due to thermal relaxation, viz. $q_m \propto t^{-\gamma}$.

3.2.2. Effect of reaction rate on morphology evolution

To appreciate the effect of polymerization on the pattern forming aspect of phase separation, similar calculations have been undertaken at various reaction rates by simply varying the rate constant, k. Fig. 6 shows the snap shots of the morphology computed at $t = 100\,000$ for the compositional order parameters (upper row) and orientational order parameters (lower) with different k values. It is apparent that the final length scale representing the asymptotic equilibrium is reduced with increasing k, i.e. the faster the reaction rate, the smaller the average length scale (i.e. domain size). This behavior is reminiscent of the domain morphology developed in the slowly cooled system to be larger than that in the rapidly quenched (or deep quench) blends.

3.2.3. Reaction at an LC poor composition

A similar lamellar structure can be obtained if polymerization were carried out at a single-phase temperature at compositions either rich or poor in LC, e.g. $\phi_1 = 0.35$ or $\phi_1 = 0.65$ at $T_R = 50$°C. Fig. 7 shows the temporal evolution of (a) the compositional order parameter and (b) the corresponding orientational order parameter for $\phi_1 = 0.35$ and $T_R = 50$°C. The temporal sequence of the emerging domain structure shows the percolation-to-cluster transition. During PIPS, the UCST coexistence curve moves toward a higher LC content and surpasses the reaction temperature at an off-critical point. The initial structure appears bicontinuous and very large. The length scale declines with the progression of the reaction, which may be attributed to the increasing UCST that makes the supercooling large. After 3000 time steps, the percolated structure gradually transform to the droplet clusters, suggesting the percolation-to-cluster transition. It is fair to infer that the PIPS at

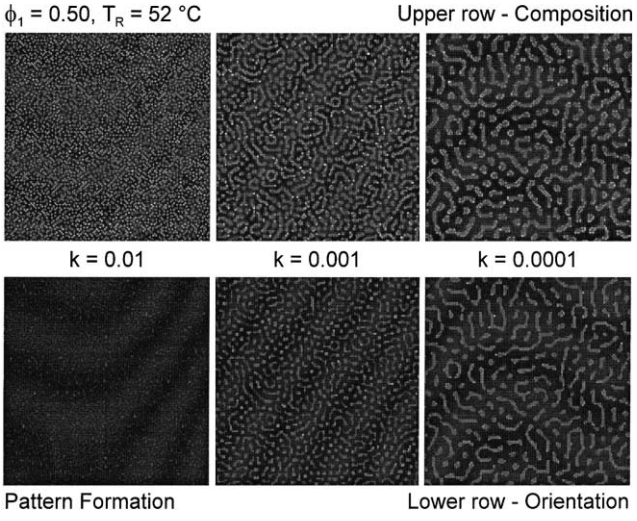

Fig. 6. Effect of the reaction rate upon the emergence of liquid crystal domains. The patterns were calculated based on the same parameters as those in Fig. 2 except $a_1 = a_2 = 0.6$ and $\kappa_s = 0.00001$. The rate constant, k, varied from 0.01 to 0.0001.

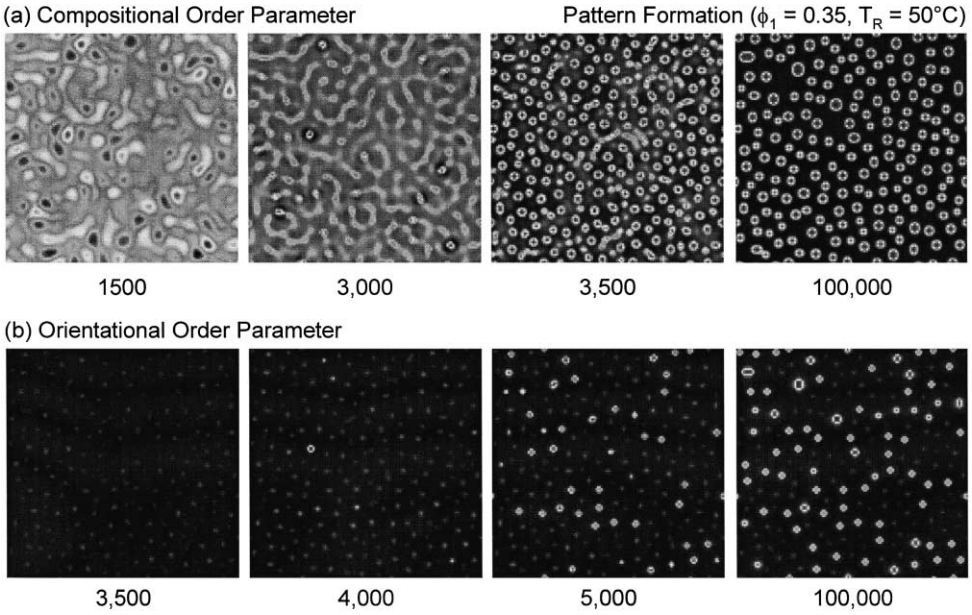

Fig. 7. Temporal evolution of (a) the compositional order parameter (upper row) and (b) the orientational order parameter (lower row) for the case $\phi_1 = 0.35$ and the reaction temperature $T_R = 50°C$. The calculation was performed using the same parameters as those in Fig. 2.

the LC poor region ($\phi_1 = 0.35$ and $T_R = 50°C$) is analogous to a far off-critical thermal quenching for which the regular droplet formation can be anticipated.

The orientational order parameter reveals no texture in the initial period of PIPS, so only the late stage data are shown in Fig. 7(b). As the LC concentration within the existing phase-separated domain increases, the directors of the LC molecules start to align among themselves and form nematics. Although the orientational ordering occurs within the phase separated domains, the nematic structure has yet to emerge, so texture can be discerned (see $t = 3000$). Only when the LC concentration exceeds the threshold value, $\phi_{NI}(t = 3500–100\,000)$, the nematic texture develop within the lamellar domains. Of particular interest is that the number of nematic droplets in the order parameter field is less than those in the concentration field simply because LCs are deficient at such low LC concentration.

3.2.4. Reaction at an LC rich composition

Fig. 8 illustrates the temporal evolution of compositional and orientational order parameter calculated for the case $\phi_1 = 0.65$ and $T_R = 50°C$. With progressive polymerization, the

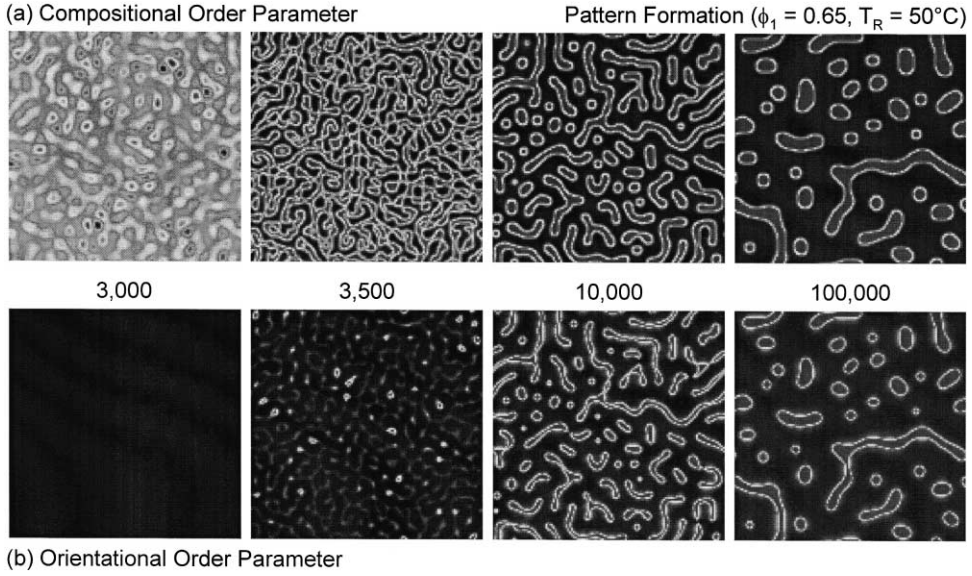

Fig. 8. Temporal evolution of the (a) the compositional order parameter (upper row) and (b) the orientational order parameter (lower row) for the case: $\phi_1 = 0.65$ and $T_R = 50°C$. Other parameters were kept the same as those in Fig. 7.

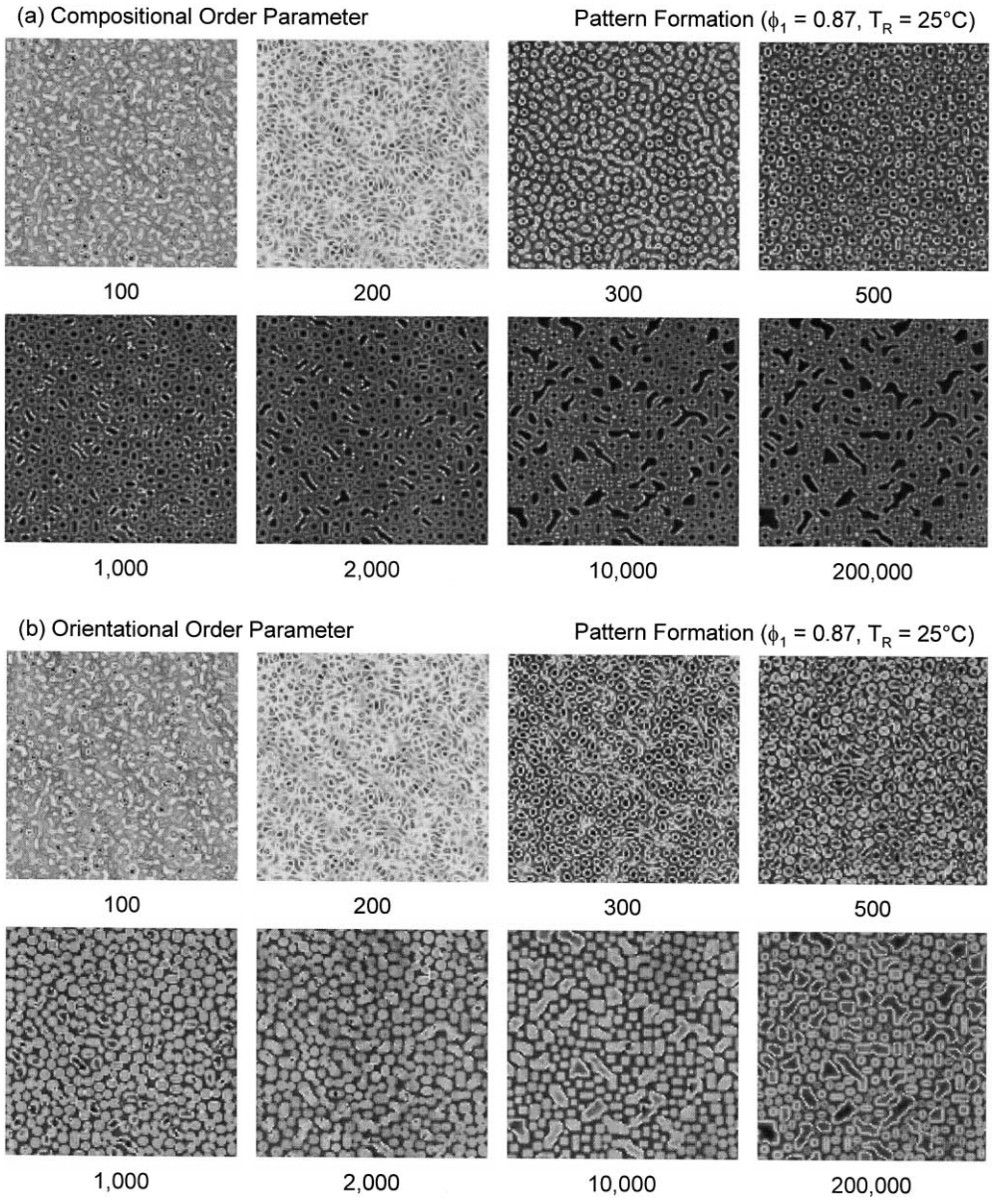

Fig. 9. Temporal evolution of (a) the compositional order parameter and (b) the orientational order parameter for the case $\phi_1 = 0.87$ and $T_R = 25$°C, showing bimodal droplets. Other parameters were the same those in Fig. 2, except $D_1 = D_2 = 0.1$.

critical UCST point shifts to a higher temperature while moving in the direction of the LC-rich compositions and it eventually surpasses the reaction temperature. This reacting blend corresponds to the off-critical composition, but it is in the direction of the asymmetric movement of the UCST. It is apparent that the concentration fluctuations first grow in magnitude via NG and later transform into a bicontinuous SD texture ($t = 1000$–5000). This interconnected structure grows through coalescence ($t = 100\,000$). As expected, LC ordering takes place within these interconnected domains. This scenario is reminiscent of the case at the critical composition of the starting mixture for which interconnected texture can be expected, as SD is prevalent in this region. The size of the domains in the orientational order parameter field is seemingly smaller than that in the compositional field. This observation is not surprising in view of the fact that the orientational order parameter must exceed a critical value, $s_c = 0.429$ in order for the nematic to form. The growth dynamic curve is not shown here since it is more or less similar to those shown for the $\phi = 0.5$ case (Fig. 5).

3.3. Reaction in a two-phase region

One interesting feature in the phase diagram (Fig. 1) is the existence of the nematic spinodal line that separates the nematic unstable and metastable states. It is therefore of interest to investigate the role of nematic spinodal line on the emergence of the LC domain morphology. We

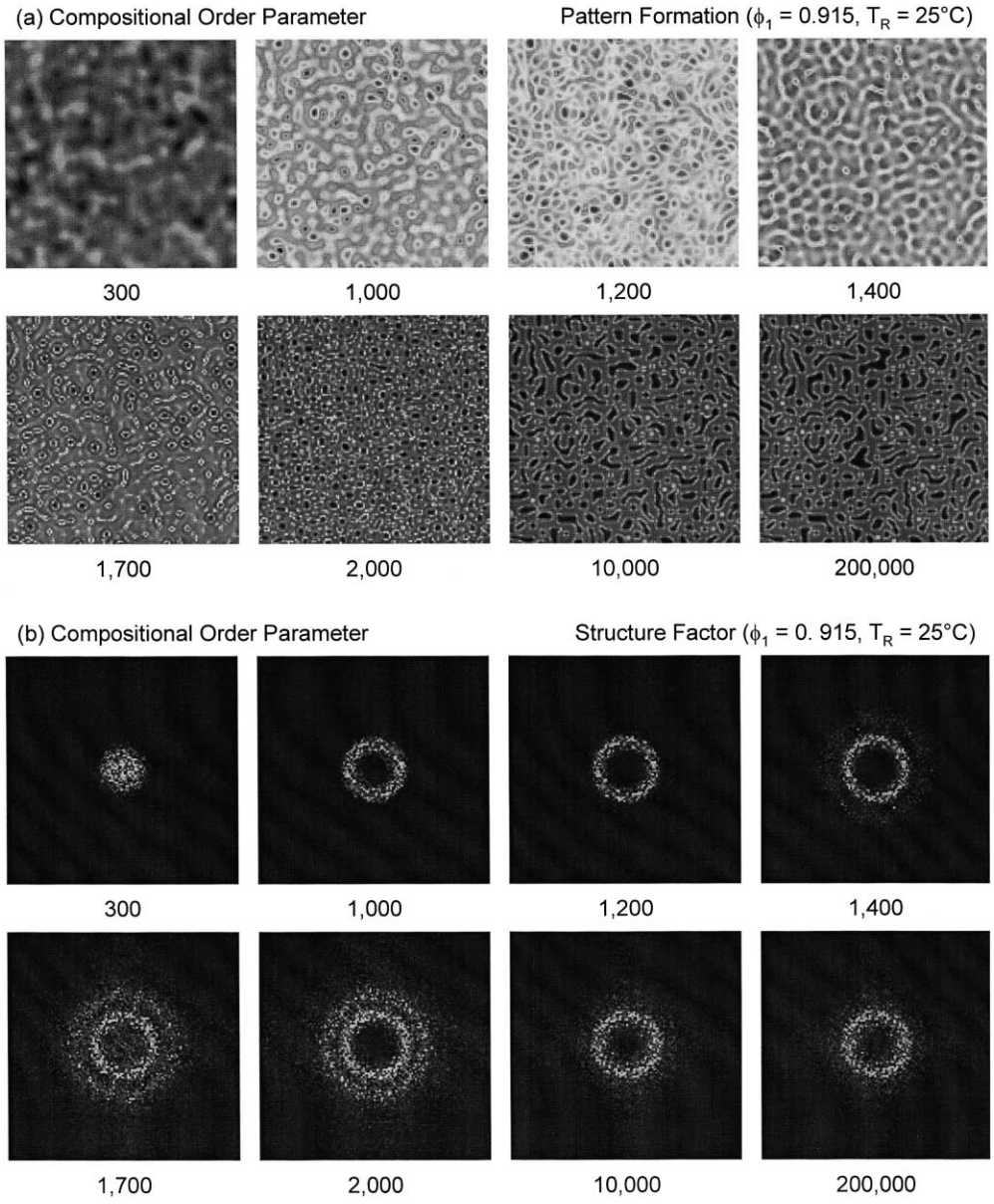

Fig. 10. Temporal evolution of (a) the compositional order parameter and (b) the corresponding FFT patterns for the case $\phi_1 = 0.915$ and $T_R = 25$°C, showing the interconnected network-like morphology. Other parameters were the same as those in Fig. 9 except the blend ratio.

simulated for two cases (i) $\phi_1 = 0.87$ and $T_R = 25$°C that corresponds to the nematic unstable region and (ii) $\phi_1 = 0.915$ and $T_R = 25$°C that corresponds to the nematic metastable, but both cases are outside of the L–L coexistence line of the starting LC/monomer mixture. When reaction is initiated, the UCST curve moves up while the nematic spinodal line moves toward a higher LC concentration. In Case (i), the reaction system follows a trajectory passing through the L–L metastable to the L–L unstable region, but it still remains in the unstable nematic region.

Fig. 9 illustrates the temporal evolution of (a) the compositional order parameter and (b) the orientational order parameter for Case (i). Tiny, but seemingly interconnected structures develop almost instantaneously in both compositional and orientational order parameter fields. The initial phase separation is probably triggered the nematic ordering since the starting mixture was in the isotropic L–L region, but in the unstable nematic region. The percolated structure transforms to cluster as the system enters the metastable L–L region, then becomes interconnected again as the system was further thrust deeper into the unstable L–L region. This complex phase change of the percolation–cluster–percolation manifests as to how the system in the unstable nematic region has undergone from the isotropic, metastable to unstable L–L states.

In Case (ii), the stating LC/monomer mixture was in the isotropic state of the L–L coexistence curve, but in the metastable nematic region. When reaction occurs, the reaction

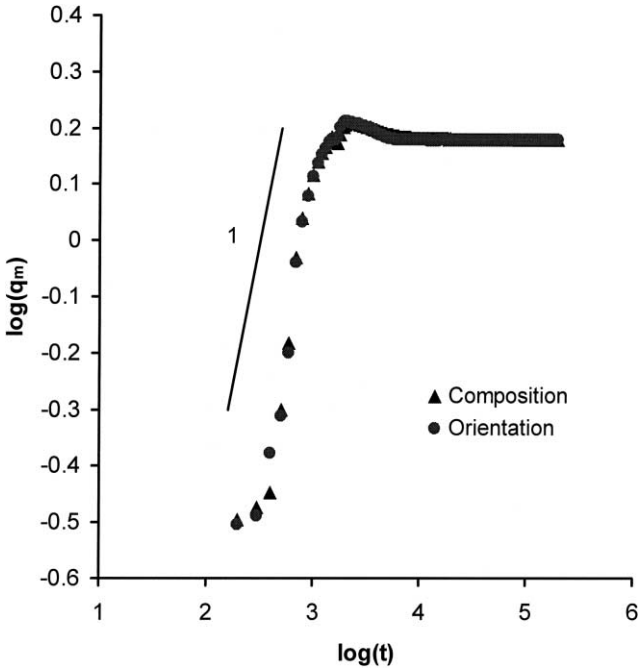

Fig. 11. $\log(q_m)$ versus $\log(t)$ plots for the compositional and orientational order parameters for the case $\phi_1 = 0.915$ and $T_R = 25°C$.

point crosses not only the L–L binodal and spinodal lines, but also the nematic spinodal line. It appears the phase separation is probably triggered by the nematic ordering within the metastable nematic region. As typical for the metastable region, small fluctuations tend to decay leaving the disproportionate amount of large fluctuations behind upon which growth occurs. So the initial texture is large (Fig. 10). With the progression of the reaction, the UCST moves up, that makes the system to enter from the isotropic to the unstable L–L region through the metastable region. Concurrently, the mixture is thrust from the metastable nematic to the unstable nematic region during PIPS. The structure tends to become interconnected when the system reaches the unstable state against both the L–L coexistence and the nematic spinodal curves. The final morphology in both compositional and orientational field shows network-like topology which is a typical structure reported for the polymer stabilized LCs [53,54].

In Fig. 10(b), the corresponding scattering halo shows no identifiable peak initially (see $t = 300$), which is a signature of the PIPS being triggered in the metastable nematic region. As the system is pushed into the unstable region, the scattering peak becomes distinct (after 1000 time steps), while the ring diameter increases, suggestive of the size reduction. In this region, the interconnected domains are seemingly unstable and tend to break-up while nematic ordering is taking place internally. In the intermediate growth region ($t = 1200$–$2,000$), a secondary peak develops at a larger angle, which may be attributed to the increased correlation of the nematic directors. In the late stages ($t = 10\,000$–$100\,000$), the outer ring diminishes while the inner ring diameter decreases slightly. Such growth characteristics may be best explained in the context of the power law.

As shown in Fig. 11, the q_m increases sharply in the initial period of the PIPS, suggestive of the reduction in length scale, which is one of the unique characteristic of PIPS. The growth curve for the orientational order parameter field is virtually overlapped with that of the composition. This observation is not surprising in view of the fact that the phase separation was triggered by the nematic ordering in the metastable nematic region, so the patterns form almost simultaneously in the compositional and orientational order parameter fields. The physical meaning of the slope of 1 is presently not understood because of the complex competition between the PIPS and TIPS. The PIPS process seems to prevail in the early stage, but the TIPS presumably becomes more dominant at late stages. This fact is manifested in the decline of the scattering wavenumber maximum due to the domain coarsening before it asymptotically levels off.

4. Conclusions

We have demonstrated that the emergence of LC domains in a PDLC prepared via polymerization induced phase separation can be well characterized by incorporating the reaction kinetics into the time-dependent Ginzburg–Landau (TDGL-Model C) equations in conjunction with the combined Flory–Huggins (FH)/Maier–Saupe (MS) theory. The TDGL equations are basically two coupled equations in which a conserved compositional order parameter (i.e. the volume fraction of the LCs) is coupled with a non-conserved orientational order parameter. It was demonstrated that the emerging LC domain morphology is profoundly affected by the movement of UCST phase diagram as well as by the nematic spinodal line during the course of PIPS. At intermediate compositions, the phase separation is characterized by the size reduction due to increasing supercooling associated with the movement of the UCST curve during the PIPS, then followed by the structural coarsening due to thermal relaxation. At the LC poor region, droplet morphology is prevalent as typical for the off-critical mixture. When polymerization is initiated in a two-phase region at an off-critical composition rich in LC, the percolation–cluster–percolation transition was found to occur as the system in the unstable nematic region drifts from the isotropic to the unstable spinodal region through the metastable region of L–L phase separation. At the higher LC concentration of $\phi_1 = 0.915$, a network-like structure developed which is consistent with the observed morphology of the polymer stabilized LCs.

Acknowledgements

The present work is made possible by the support from the National Science Foundation through Grant Number

DMR 95-29296, DMR 99-03519 and NSF-STC: Advanced Liquid Crystal Optical Materials (ALCOM) Grant Number 89-20147 and Ohio Board of Regents Research Challenge Grant.

References

[1] Doane JW. In: Bahadur B, editor. Liquid crystals: applications and uses. Singapore: World Scientific, 1990. p. 361, chapter 14.
[2] Drzaic PS. Liquid crystal dispersions. Singapore: World Scientific, 1995.
[3] West JL. In: McKay RB, editor. Technological applications of dispersions. New York: Marcel Dekker, 1994. p. 345.
[4] Gunton JD, San Miguel M, Sahni PS. In: Domb C, Lebowitz JL, editors. Phase transitions and critical phenomena. New York: Academic Press, 1983.
[5] Chaikin PM, Lubensky TC. Principles of condensed matter physics. New York: Cambridge University Press, 1995.
[6] Shen C, Kyu T. J Chem Phys 1995;102:556.
[7] Chiu H-W, Kyu T. J Chem Phys 1995;103:7471.
[8] Chiu H-W, Zhou ZL, Kyu T, Cada LG, Chein LC. Macromolecules 1996;29:1051.
[9] Kyu T, Chiu H-W. Phys Rev E 1996;53:3618.
[10] Chiu H-W, Kyu T. J Chem Phys 1997;107:6859.
[11] Chiu H-W, Kyu T. J Chem Phys 1998;108:3249.
[12] Flory PJ. Principles of polymer chemistry. Ithaca: Cornell University Press, 1953.
[13] Olabisi O, Robeson LM, Shaw MT. Polymer–polymer miscibility. New York: Academic Press, 1979.
[14] Maier W, Saupe A. Z Naturforsch 1959;Teil A 14:882.
[15] Maier W, Saupe A. Z Naturforsch 1960;15:287.
[16] de Gennes PG, Prost J. The physics of liquid crystal. 2nd ed. London: Oxford Scientific Publications, Oxford University Press, 1993.
[17] McMillan WL. Phys Rev A 1971;4:1238.
[18] Kim JY, Cho CH, Palffy-Muhoray P, Mustafa M, Kyu T. Phys Rev Lett 1993;71:2232.
[19] Lin J-C, Taylor PL. Mol Cryst Liq Cryst 1993;237:25.
[20] Glotzer SC, Coniglio A. Phys Rev E 1994;50:4241.
[21] Glotzer SC, Coniglio A. Phys Rev Lett 1995;74:2034.
[22] Jin J-M, Parbhakar K, Dao LH. Comput Mater Sci 1995;4:59.
[23] Kyu T, Lee JH. Phys Rev Lett 1996;76:3746.
[24] Chiu H-W, Lee JH, Kyu T. In: Rozenberg BA, Sigalov GM, editors. Cure reaction induced phase separation in polymer blends. 2001, in press.
[25] Chan PR, Rey AD. Macromolecules 1996;29:8934.
[26] Fukuda J. Phys Rev E 1998;58:6939.
[27] Fukuda J. Phys Rev E 1999;59:3275.
[28] Brochard F, Jouffroy J, Levinson P. J Phys 1984;45:1125.
[29] Palffy-Muhoray P, de Bryun JJ. Mol Cryst Liq Cryst 1985;127:301.
[30] Liu AJ, Fredrickson G. Macromolecules 1992;25:5551.
[31] Matsuyama A, Kato T. Phys Rev E 1998;58:585.
[32] Matsuyama A, Kato T. J Chem Phys 1998;109:2023.
[33] Benmounna F, Coqueret X, Maschke U, Benmounna M. Macromol Theory Simul 1998;7:599.
[34] Benmounna F, Coqueret X, Maschke U, Benmounna M. Macromolecules 1998;7:4879.
[35] Dorgan JR. J Chem Phys 1993;98:9094.
[36] Dorgan JR, Yan D. Macromolecules 1998;31:193.
[37] Lin Z, Zhang H, Yang Y. Macromol Theory Simul 1997;6:1153.
[38] Lapena A, Glotzer SC, Langer SA, Liu AJ. Phys Rev E Rapid Commun 1999;60:R29–32.
[39] Fukuda J. Phys Rev E Rapid Commun 1998;58:R6939.
[40] Fukuda J. Phys Rev E 1999;59:3275.
[41] Chiu H-W, Kyu T. J Chem Phys 1999;110:5998.
[42] Nwabunma D, Chiu H-W, Kyu T. J Chem Phys 2000;113:6429.
[43] Kyu T, Ilies I, Mustafa M. J Phys IV 1993;3:37.
[44] Kyu T, Ilies I, Shen C, Zhou ZL. In: Isayev AI, Kyu T, Cheng SZD, editors. Liquid crystalline polymer systems: technological advances, ACS Symposium Series #632. Washington, DC: ACS, 1996. p. 201, chapter 13.
[45] Odian G. Principles of polymerization. New York: Wiley-Interscience, 1981.
[46] Inoue T. Reaction-induced phase decomposition in polymer blends. Prog Polym Sci 1995;20:119.
[47] Yamanaka K, Takagi Y, Inoue T. Polymer 1989;30:1839.
[48] Ohnaga T, Chen W, Inoue T. Polymer 1994;35:3774.
[49] Ryan ME, Dutta A. Polymer 1979;20:203.
[50] Takenaka M, Hashimoto T. Phys Rev E 1993;48:47.
[51] Doi M, Edwards SF. Theory of polymer dynamics. New York: Academic Press, 1986.
[52] Binder K. J Chem Phys 1983;79:6387.
[53] Rajaram CV, Hudson SD, Chien LC. Chem Mater 1995;7:2300.
[54] Rajaram CV, Hudson SD, Chien LC. Chem Mater 1996;8:2451.